



Multi-year high time resolution measurements of fine PM at 13 sites of the French Operational Network (CARA program): Data processing and chemical composition

5 Hasna Chebaicheb^{1,2,3}, Joel F. de Brito^{1,3}, Tanguy Amodeo^{2,3}, Florian Couvidat², Jean-Eudes Petit⁴, Emmanuel Tison^{1,3}, Gregory Abbou⁵, Alexia Baudic⁵, Mélodie Chatain⁶, Benjamin Chazeau^{7,8}, Nicolas Marchand⁸, Raphaële Falhun⁹, Florie Francony¹⁰, Cyril Ratier¹⁰, Didier Grenier¹¹, Romain Vidaud¹¹, Shouwen Zhang¹², Gregory Gille^{1,3}, Laurent Meunier^{2,3}, Caroline Marchand^{2,3}, Véronique Riffault^{1,3}, Olivier Favez^{2,3}

10 ¹IMT Nord Europe, Institut Mines-Télécom, Université de Lille, Centre for Energy and Environment, 59000, Lille, France

²Institut National de l'environnement Industriel et des Risques (INERIS), 60550 Verneuil-en-Halatte, France

³Laboratoire Central de Surveillance de la Qualité de l'Air (LCSQA), 60550 Verneuil-en-Halatte, France

15 ⁴Laboratoire des Sciences du Climat et de l'Environnement (LSCE), CNRS-CEA-UVSQ (UMR 8212), 91191 Gif-sur-Yvette, France

⁵Airparif, Air Quality Monitoring Network for the Greater Paris Area, 75004 Paris, France

⁶Atmo Grand Est, 67300 Schiltigheim, France

⁷Laboratory of Atmospheric Chemistry, Paul Scherrer Institute, 5232 Villigen, Switzerland

⁸Aix Marseille Univ, CNRS, LCE, Marseille, France

⁹Air Breizh, 35200 Rennes, France

20 ¹⁰Atmo Nouvelle-Aquitaine, 33692 Mérignac, France

¹¹Atmo Auvergne Rhône-Alpes, 69500 Bron, France

¹²Atmo Hauts-de-France, 59800 Lille, France

¹³AtmoSud, Regional Network for Air Quality Monitoring of Provence-Alpes-Côte-d'Azur, Marseille, France

25 *Correspondence to:* hasna.chebaicheb@ineris.fr

Abstract. This paper presents a first comprehensive analysis of long-term measurements of atmospheric aerosol components from Aerosol Chemical Speciation Monitor (ACSM) and multi-wavelength Aethalometer (AE33) instruments collected between 2015 and 2021 at 13 (sub)urban sites as part of the French CARA program. The datasets contain the mass concentrations of major chemical species within PM₁, namely organic aerosols (OA), nitrate (NO₃⁻), ammonium (NH₄⁺), sulfate (SO₄²⁻), non-sea-salt chloride (Cl⁻), and equivalent black carbon (eBC). Rigorous quality control, technical validation, and environmental evaluation processes were applied, adhering to both the guidance from the French reference laboratory for air quality monitoring and the Aerosol, Clouds, and Trace gases Research Infrastructure (ACTRIS) standard operating procedures. Key findings include geographical differences in aerosol chemical composition, seasonal variations, and diel patterns, which are influenced by meteorological conditions, anthropogenic activities, and proximity to emission sources. Overall, OA dominates PM₁ at each site (43-60 %), showing distinct seasonality with higher concentrations (i) in winter, due to enhanced residential heating emissions, and (ii) in summer, due to increased photochemistry favoring secondary aerosol formation. NO₃ is the second most important contributor to PM₁ (15-30 %), peaking in late winter and early spring, especially in northern France, and playing a significant role during pollution episodes. SO₄ (8-14 %) and eBC (5-11%) complement the major fine aerosol species, with their relative contributions strongly influenced by the origin of air masses and the stability of meteorological conditions, respectively.

30
35
40



- Such chemically-speciated multi-year datasets have significant value for the scientific community, offering opportunities for future research, including source apportionment studies, trend analyses, and epidemiological investigations. They are also vital for evaluating and validating regional air quality models. In this regard, a comparison with the CHIMERE Chemical Transport Model shows high correlations between simulations and measurements, albeit underestimating OA concentrations by 46-76 %. Regional discrepancies in NO₃ concentration levels emphasize the importance of these datasets in validating air quality models and tailoring air pollution mitigation strategies.
- 45
- 50 **Keywords.** Urban pollution, ACSM, AE33, equivalent black carbon eBC, non-refractory submicron aerosols NR-PM₁, Chemical composition, France, chemical transport model/modeling



1 Introduction

The investigation of atmospheric aerosols holds significant importance in both the scientific and policy spheres due to their substantial impacts on climate (IPCC, 2021) and human health (WHO, 2021). In Europe, for instance, it is estimated that in 2021, 97 % of the urban population experienced levels surpassing the annual concentration of $5 \mu\text{g m}^{-3}$ recommended by the World Health Organization (WHO) for particulate matter with an aerodynamic diameter smaller than $2.5 \mu\text{m}$ ($\text{PM}_{2.5}$), and exposure to these fine particles was associated in 2021 with more than 253,000 premature deaths (EEA, 2023). WHO guidelines as well as regulatory thresholds set at the national level (according to the Directive 2008/50/EC for European Member States) are mainly linked with the total mass concentration of suspended particles in a given size range. However, the elaboration and evaluation of specific action plans to improve air quality require a sound knowledge of their formation, which also allows the investigation of their emission sources and chemical processes in ambient air (Viana et al., 2008, Fuzzi et al., 2015). Moreover, forecasting systems, such as those using Chemical Transport Models (CTMs), usually use chemically-speciated emission inventories as inputs, and their validation benefits from comparisons with measurements of the PM chemical composition at representative sites (e.g., Ciarelli et al., 2016, EMEP, 2022).

Historically, PM chemical speciation was mainly based on offline laboratory analyses of aerosol samples collected on filters (e.g., Putaud et al., 2004). Such methods are nowadays well standardized and provide the opportunity for comprehensive characterization of major species as well as trace compounds (EMEP, 2022). However, they are known to be subject to various sampling artifacts (Schaap et al., 2004; Wittmaack and Keck, 2004) and are collected at relatively low temporal resolution (typically 24h). They are also quite laborious and costly when used for long-term monitoring purposes. To overcome these limitations, significant efforts have been made to develop online chemical analyzers for in situ measurements in near real time. In particular, there has been a growing interest in the continuous quantification of black carbon in ambient air, especially using filter-based absorption photometers (Savadkoobi et al., 2023), given the significant influence of this aerosol component on climate (Jacobson et al., 2001). In parallel, the development and worldwide deployment in the last two decades of the Aerosol Mass Spectrometer (AMS, Canagaratna et al., 2007) has allowed studying non-refractory compounds (i.e., organic aerosol (OA), nitrate (NO_3^-), sulfate (SO_4^{2-}), chloride (Cl^-), and ammonium (NH_4^+)) within the fine aerosol mode (mainly PM_{10}) (Crenn et al., 2017, Lanz et al., 2010, Roig Rodelas et al., 2019, Sun et al., 2010, Zhang et al., 2017). In addition to these sophisticated high-resolution instruments, which are well suited for intensive but short-term campaigns, the Aerosol Chemical Speciation Monitor (ACSM) has been designed for continuous, multiannual measurements of the same major chemical species in the PM_{10} or $\text{PM}_{2.5}$ fractions (Bressi et al., 2021; Chebaicheb et al., 2023; Heikkinen et al., 2021; Ng et al., 2011; Zhang et al., 2019). Both measurement methods (i.e., absorption photometers and ACSM) have become widely used in research monitoring, such as the Aerosol, Clouds, and Trace gases Research Infrastructure (ACTRIS, www.actris.eu) in Europe (Laj et al., 2024), and within the Atmospheric Science and mEasurement NeTwork (ASCENT, <https://research.gatech.edu/>) in the United States. Their robustness and relatively low operating costs also make them good candidates for deployment at air quality monitoring stations operated by environmental agencies (Petit et al., 2015).

In this context, since 2015, multi-wavelength Aethalometers (AE33 model, Drinovec et al., 2015) and ACSM instruments have been operated at an increasing number of urban sites in France as part of the CARA program within the national air quality monitoring network (Favez et al., 2021), with the following main objectives: (i) to



document in near real time the chemical composition (and possibly the dominant sources) of PM pollution episodes; (ii) to provide multi-year datasets of the chemical composition of the fine PM fraction, to be included into future trend analyses and/or epidemiological studies; (iii) to provide a comprehensive overview of the temporal and spatial variability of the chemical composition of fine PM over France, which can contribute in particular to evaluating and improving the accuracy of air quality models.

The main objective of this paper is to report on the chemically-specified datasets and major findings obtained so far from these observations. After describing the quality control procedures applied to the corresponding measurements, we investigate the geographical specificities exhibited by the main chemical species within the fine PM and then provide typical seasonal and diel variations displayed by these compounds in France over the period 2015-2021. The datasets presented here are made fully available for complementary research activities, including the evaluation of the accuracy of CTMs through comparison exercises, examples of which are also discussed in this article.

2 Methodology

2.1 Sites and measurement periods

The current study presents the chemical composition of fine particles within the CARA program during the period 2015-2021, at 13 sites in France, including 11 stations from regional air quality monitoring networks (AASQAs), as well as two research platforms - i.e., SIRTAs (Greater Paris area) and ATOLL (Lille metropolis) - both of which are also part of the ACTRIS European research infrastructure. These stations have been gradually equipped with AE33 and ACSM instruments from 2015 onwards. A detailed description of these instruments is given in the next section, and the temporal coverage of the measurements considered here for each site is presented in Figure 1. A summary of each sampling site, including coordinates and related networks, can also be found in the Supplementary Information, Table S1. The majority of these sites are urban background sites, with the exception of two suburban sites (ATOLL and SIRTAs) and one urban traffic site (Boulevard Périphérique Est; BPEst in Paris). Geographically distributed throughout France, these sampling sites provide a global view of the chemical composition of fine particles at the national scale.



Figure 1: ACSM and AE33 measurement periods considered for each site in this study.

120 2.2 Non-refractory submicron aerosol measurements

2.2.1 ACSM measurement principles

The ACSM, developed by Aerodyne Research Inc., is based on mass spectrometry. As previously mentioned, it measures the chemical composition of NR-PM₁ in real-time, allowing long-term measurements with less monitoring and technical intervention compared to AMS, and a relatively high temporal resolution of about 30 minutes (Watson, 2017). All stations presented in this study are equipped with Quadrupole ACSMs (Q-ACSM, Ng et al., 2011), except for the Marseille-Longchamp site, where a Time-of-flight ACSM (ToF-ACSM, Fröhlich et al., 2013) is deployed. The Q-ACSM is the most commonly used analyzer because it meets the operational monitoring needs of the French monitoring agencies and is less complex than the ToF-ACSM, although the latter has lower detection limits and slightly better time resolution (about 10 minutes).

130 The operating principle of the ACSM is briefly described below. Ambient air first enters the vacuum system through a 100 μm diameter critical orifice. It then passes through an aerodynamic lens that focuses the aerosol into a concentrated beam, which is further directed onto a vaporizer heated at a temperature of about 600°C, causing the particles to transition to the gas phase. The gas phase molecules are then subjected to ionization at 70 eV, resulting in molecular fragmentation. The fragmented ions are guided by ion lenses to a quadrupole or time-of-flight mass filter, depending on the ACSM model.

135 In the ACSM, the atmospheric sample is analyzed alternatively by passing or not through a particulate filter. The air signal can thus be subtracted from the unfiltered measurements to quantify the particulate chemical species. A measurement timebase of approximately 29 min (corresponding to 28 cycles of filtered/unfiltered atmospheric



140 samples) was used for each Q-ACSM dataset, while data were acquired with a 10 min timebase for the ToF-ACSM. All ACSMs operated under the CARA program were equipped with a PM₁ aerodynamic lens and a standard vaporizer.

145 In the measured mass spectra, each m/z fragment is linked to one or more species based on a fragmentation table originally developed by Allan et al. (2004) and subsequently refined by Canagaratna et al. (2007). The concentration of each chemical species is then obtained as the sum of its contribution in every corresponding m/z fragment. Moreover, the instrument-specific response factor (RF) of NO₃ and the relative ionization efficiencies (RIE) of NH₄ and SO₄ are determined by sampling 300 nm ammonium nitrate (NH₄NO₃) and ammonium sulfate ((NH₄)₂SO₄) aerosols (Freney et al., 2019). For OA and CI, the default RIE values of 1.4 and 1.3 are used here. Finally, to obtain quantitative mass concentrations for each measured chemical species, a collection efficiency (CE) correction factor is applied, following the procedure proposed by Middlebrook et al. (2011).

150 2.2.2 ACSM quality checks and data handling

The data collected here from the ACSM instrument follows strict quality control and technical validation, including an environmental evaluation involving comparison with complementary data. It has been performed following the guidance provided by the French reference laboratory for air quality monitoring (LCSQA, 2018) and in full agreement with the ACTRIS standard operating procedures, which are available online (<https://www.actris-ecac.eu/pmc-non-refractory-organics-and-inorganics.html>).

155 On-site calibrations for air quality monitoring sites have been performed yearly by LCSQA personnel as well as after each sensitive maintenance by the instrument distributor in Europe (ADDAIR). A detailed description of the applied calibration procedures is available in a specific document edited at the national level (LCSQA, 2022). Moreover, each ACSM of the CARA program has routinely participated in intercomparison exercises organized by the Aerosol Chemical Monitor Calibration Centre (ACMCC) at SIRT, to ensure proper calibration and functioning of the instruments (e.g., LCSQA, 2023).

160 Given the majority of instruments used here are Q-ACSM, data processing will be detailed focusing on this model. ToF-ACSM data processing (deployed at Marseille-Longchamps) is described more specifically in Chazeau et al. (2021). The Q-ACSM data handling was carried out using the manufacturer's software in Igor Pro Version 6.37.

165 The first step involved checking the stability and continuity of technical parameters, including inlet pressure (maintained at approximately 1.3 ± 0.2 torr), vaporizer temperature (regulated from the voltage calibration curve initially defined by the manufacturer), Secondary Electron Multiplier (SEM) and Heater Bias voltages, filament emission, airbeam value (set around $10^7 \pm 30\%$ ions/s), and relative humidity (ensuring it remains below 40 % using a Nafion dryer upstream the inlet). Data points exhibiting inconsistencies were systematically flagged and invalidated. Secondly, the calibration results, notably the RF and RIE, were carefully analyzed for consistency. This approach ensured that the data cleaning process was attuned to changes in RF and RIE, thereby improving the accuracy of the resulting dataset. If the RIE and RF values from two subsequent calibrations were deemed comparable, their average was used. Otherwise, time-dependent RIE and RF were used, notably following instrument modification. During this data cleaning phase, the CE was maintained at a constant value of 1. Thirdly, 175 data points with air (m/z 28, 32, and 40) and water (m/z 18) signal spikes were removed through a systematic cleaning procedure executed within the Igor Pro software, which allows the removal of signals that appear



anomalous. This step also entails a comprehensive analysis of other ions to capture additional insights from the data. In particular, the examination of ions associated with chloride (m/z 35 and 36) allows for checking any possible measurement artifact that may be caused by sea salts (Tobler et al., 2020), while specific organic compounds (m/z 43, 44, and 55), including the fragment related to levoglucosan (m/z 60), serve as a crucial checkpoint for assessing the impact of distinct sources, such as biomass combustion, traffic emissions and/or secondary formation processes.

As a next step, the implementation of the TIS (*Time series*) and RIT (*Relative Ion Transmission*) corrections were performed. The TIS correction encompasses the correction of crucial time-dependent signals that exert a significant influence on the measured concentrations captured by the instrument. These include the adjustment of variables such as the inflow rate directed into the Q-ACSM 'reference P' (inlet pressure), the 'reference N2' signal for airbeam, and the 'reference RF' for ionization efficiency. Subsequently, the RIT correction is applied to account for the mass spectrometer transmission efficiency within the Q-ACSM, based on the naphthalene peaks used as internal standard and represented by m/z 51, 62, 76, 102, and 128 (normalized to 1 below m/z 51 and set at 0.05 for m/z 154 and beyond with an exponential fit for the interval in between). We also closely examined the RIT time series linked to these ions, particularly in cases where the RIT standard deviation was high. We found several instances where the mean RIT value may appear satisfactory, yet the time series could have periods of anomalous behavior. Thus, it is essential to carefully examine each time series of individual naphthalene masses, beyond the evaluation of average RIT values alone. After these corrections, the Middlebrook algorithm (Middlebrook et al., 2011), with a minimum CE of 0.5, was applied to correct the mass concentrations for the so-called composition-dependent collection efficiency (CDCE) correction.

The following verification step involves examining the ion balance, which implies assessing the correlation between the measured and predicted NH_4 concentrations, with a target slope theoretically falling within the range of $1 \pm 10\%$, at sites and under atmospheric conditions where most aerosols should contain enough ammonium to be neutral as ammonium nitrate NH_4NO_3 , ammonium sulfate $(\text{NH}_4)_2\text{SO}_4$ and ammonium chloride NH_4Cl . To compute the measured and predicted NH_4 concentrations, the following calculations were employed:

$$\text{NH}_{4,\text{measured}} = \frac{[\text{NH}_4]}{18} \quad (1)$$

$$\text{NH}_{4,\text{predicted}} = \frac{[\text{NO}_3]}{62} + 2 \frac{[\text{SO}_4]}{96} + \frac{[\text{Cl}]}{35.45} \quad (2)$$

Finally, the analysis carefully accounted for the specific detection limits (DL) corresponding to various chemical species. Following Ng et al. (2011a), DL values for Q-ACSM are 0.284, 0.148, 0.024, 0.012, and $0.011 \mu\text{g m}^{-3}$ for NH_4 , OA, SO_4 , NO_3 , and Cl, respectively. The same DL has been considered here for the ToF-ACSM instrument deployed in Marseille-Longchamp. Data levels above the DL were validated, whereas those between $-3 \times \text{DL}$ and DL were replaced by $\text{DL}/2$. Conversely, data below $-3 \times \text{DL}$ were invalidated (Table S2).



210 2.3 Equivalent Black Carbon measurements

2.3.1. Brief description of the AE33 device

215 Complementary to ACSM measurements, equivalent black carbon (eBC) has been monitored at all sites over the same periods using a multi-wavelength Aethalometer model AE33 (Magee Scientific). As with other filter-based absorption photometers, the AE33 primarily determines aerosol absorption coefficients (b_{abs}) at selected wavelengths, based on the rate of change in the attenuation of light transmitted through the particle-laden filter. A full description of the AE33 operating principles is given by Drinovec et al. (2015). Briefly, the instrument continuously captures aerosol particles by directing the airflow onto a specific spot on the filter tape. It assesses the aerosol by gauging the amount of light transmission that passes through a part of the filter tape containing the sample, compared to the light passing through a reference zone. In the AE33, the reference zone also samples aerosols albeit with a reduced airflow, thus at different aerosol accumulation rates, allowing for more accurate eBC and particle light absorption estimates (termed ‘dual spot’). The analysis is carried out at seven optical wavelengths ranging from near-ultraviolet (UV) to near-infrared (IR) (370, 470, 525, 590, 660, 880, and 950 nm).

220 It should be noted that AE33 measurements used in the present paper have been performed in the PM_{10} fraction at both ACTRIS national facilities (ATOLL and SIRTA) but in the $PM_{2.5}$ fraction at other stations. It is however considered that black carbon aerosols are overwhelmingly present in submicron particle matter (Bond et al., 2013) so that eBC concentrations discussed herewith can be (i) compared together (i.e., from one site to another), and (ii) combined with ACSM NR- PM_{10} measurements to describe the main chemical components of fine PM at the studied sites.

2.3.2. AE33 quality checks and data handling

230 Similarly to ACSM measurements, the AE33 devices were operated following the LCSQA guidelines (LCSQA, 2020). The absorption coefficients used herewith were then calculated at each wavelength according to current ACTRIS guidelines (<https://actris-ecac.eu/particle-light-absorption.html>), following Eq. (3):

$$b_{abs} = \frac{eBC \times MAE}{H} \quad (3)$$

235 where MAE represents the specific mass absorption efficiency corresponding to each wavelength (empirically determined by the manufacturer), and H is the appropriate harmonization factor to account for multiple scattering effects of the filter, which is set at 1.76 for AE33 devices using the M8060 filter tape. The eBC concentrations were then derived by normalization with a constant mass absorption cross-section (MAC_{ACTRIS}) recently investigated in the frame of the H2020 RI-URBANS EU research program (Alastuey et al., 2022; Savadkoobi et al., 2023), following Eq. (4):

$$240 \quad eBC = \frac{b_{abs}}{MAC_{ACTRIS}} \quad (4)$$

eBC concentrations are obtained at a wavelength of 880 nm, which is recommended for black carbon measurements. This is because it is less prone to artifacts caused by other light-absorbing compounds such as dust and organic compounds (notably iron oxides and brown carbon, BrC, which absorb light at shorter wavelengths in the UV spectrum). At 880 nm, the MAC_{ACTRIS} factor used here is equivalent to $7.5 \text{ m}^2 \text{ g}^{-1}$, also in good agreement



245 with results previously obtained by Zanatta et al. (2016). It should be noted nonetheless that the application of the harmonization factor and the subsequent recalculation of eBC using a MAC comparable to the one applied by the manufacturer results in a 41% reduction in eBC levels compared to instrument output and recent studies (e.g. Chen et al., 2022).

250 AE33 data qualification procedures include checking the AAE value obtained from the seven wavelengths for each data point, aggregated to a 15 min time base. Lower and upper acceptable AAE values of 0.7 and 3.0 are considered here, and the determination coefficient (r^2) of the exponential fit used to calculate this AAE value must be greater than 0.9. Datapoints that did not meet these criteria were discarded. The carefully validated data also underwent a thorough assessment against the instrumental DL, which was set at approximately 100 ng m^{-3} . Data falling within the range of $-3 \times \text{DL}$ to DL were replaced by $\text{DL}/2$, and data below $-3 \times \text{DL}$ were invalidated (Table S2).

255 The source apportionment of ambient eBC concentrations is based on the model of Sandradewi et al., (2008). Briefly, the two-component model calculates the aerosol optical absorption coefficient by combining fractions associated with wood burning (wb) and fossil fuel (ff) combustion. It exploits the variations in absorption characteristics at different wavelengths. This method is based on the assumption that wood combustion has a marked absorption in the UV (high AAE) compared with fossil fuels (low AAE). For this study, and the different sites, the separation between eBC_{ff} and eBC_{wb} was performed using the values provided by the AE33 manufacturer: AAE_{ff} = 1 and AAE_{wb} = 2 (Drinovec et al., 2015).

2.4 Chemical mass closure

265 PM₁ mass was reconstructed from combining chemical species from ACSM (NR-PM₁ = OA + NO₃ + SO₄ + NH₄ + Cl) and eBC from AE33 (PM₁ = NR-PM₁ + eBC). For each station over the study period, PM₁ mass concentrations were compared with continuous PM_{2.5} measurements conducted using a tapered element oscillating microbalance equipped with the filter dynamic measurement system (TEOM-FDMS; Thermo Fisher Scientific) and/or a FIDAS 200 optical particle counter (Palas GmbH) and/or a β gauge monitor (BAM 1020; MET ONE), according to the European standard for PM regulatory measurements (EN 16450).

270 Linear regressions of hourly data reveal fairly good agreement between the reconstructed PM₁ and the PM_{2.5} mass concentrations measured at each site (Figure S1), with determination coefficients (r^2) ranging from 0.72 to 0.88 (except for Marseille-Longchamp, which yielded an r^2 value of 0.58) and slopes varying from 0.71 to 0.99 (except for Lyon, Strasbourg, and Metz, which showed distinct lower slopes of 0.57, 0.58, and 0.61, respectively). These results confirm that PM_{2.5} are predominantly made up of submicron particles and underscore the ACSM efficacy in capturing a significant proportion of that fraction at most sites. Hereafter, PM₁ (mass concentration) will be used to refer to submicron aerosol loadings estimated as the sum of eBC and NR-PM₁ species measured by the AE33 and ACSM, respectively.

2.5 The CHIMERE model

280 In order to compare the PM₁ species measurements and results obtained with a CTM, 3D simulations were performed from a recent version of the CHIMERE model (Menuet et al. 2021) coupled with the SSH-aerosol v1.3



aerosol model (Sartelet et al., 2020). One important feature of SSH-aerosol consists in the computation of gas-particle partitioning with the thermodynamic module SOAP (Couvidat et al., 2015). This model accounts for the condensation of semivolatile organic compounds onto the organic and aqueous phases of particles as well as the effect on partitioning of interactions between organic and inorganic compounds based on their molecular structure.

285 Thermodynamic equilibrium was assumed for gas-particle partitioning.

The Secondary Organic Aerosol (SOA) mechanism of Wang et al., (2024) was used. This mechanism was obtained by using the GENOA (*GENerator of reduced Organic Aerosol*) v2.0 algorithm (Wang et al., 2022, 2023) in order to reduce the SOA mechanisms for monoterpenes and sesquiterpenes from the Master Chemical Mechanism (Saunders et al., 2003) coupled with PRAM (in order to account for SOA formation from monoterpenes by auto-oxidation) (Roldin et al., 2019). Following Wang, (2023), the hydrophilic/hydrophobic organics (Chrit et al., 2017) mechanism was used for other precursors. Primary organic aerosols are treated as semivolatile organic compounds that partition as a function of environmental conditions and can undergo ageing (Couvidat et Bessagnet 2021).

290

Boundary conditions were taken from CAMS CIFS global model simulations (Flentje et al., 2021). Meteorological data were obtained from the operational analysis of the Integrated Forecasting System (IFS) model of the European Centre for Medium-Range Weather Forecasts (ECMWF) (Flentje et al., 2021). Anthropogenic emissions of gases and particles were taken from the CAMS-REG-AP inventory (version v5.1_REF2.1) (Kuenen et al., 2022).

295

3 Results

3.1 Geographical specificities in the chemical composition

Figure 2 summarizes the PM_1 average values, as well as their relative contributions as pie charts and barplots, calculated according to the PM_1 percentiles at various sites in France.

300

The mean PM_1 concentrations at the 13 sites range from 6.8 to 16.0 $\mu g m^{-3}$, reflecting the specificities of each urban site. These levels are comparable with the annual average NR- PM_1 levels reported by Bressi et al., (2021) across 21 sampling sites in Europe (from 2.8 to 14 $\mu g m^{-3}$, including remote mountain sites), with the highest NR- PM_1 concentrations observed in mid-latitude Europe. In addition, Chen et al., (2022) reported an average PM_1 concentration of $12.2 \pm 9.3 \mu g m^{-3}$ for 13 urban sites in Europe. In the present study, PM_1 averaged $9.4 \pm 8.3 \mu g m^{-3}$ and $PM_{2.5}$ $11.5 \pm 9.2 \mu g m^{-3}$. It is important to note that this multi-year $PM_{2.5}$ level exceeds the annual WHO guideline value of 5 $\mu g m^{-3}$ for $PM_{2.5}$ (WHO, 2021), as is the case at most sites in Europe (EEA, 2021).

305

Figure 3 further displays some key statistics on the various chemical species as well as for PM_1 and $PM_{2.5}$ mass concentrations, as a function of mean levels measured at each site. The only site with a “Road-Traffic” typology (BPEst), located on the east side of the Paris ring road, exhibits the highest mean PM_1 concentration (16.0 $\mu g m^{-3}$), standing out notably on eBC, SO_4 , and OA levels (Fig. 3). On the other hand, Rennes and Strasbourg display the lowest mass concentrations of PM_1 (6.8 $\mu g m^{-3}$), both having the lowest levels of OA (around 3.5 $\mu g m^{-3}$). In addition, the site in Rennes shows a significantly lower mean eBC level (0.4 $\mu g m^{-3}$), compared to the general average (0.8 $\mu g m^{-3}$), thus depicting a lower influence of combustion aerosols at this site. The remaining sites generally exhibit a fairly homogeneous PM_1 mass concentration, ranging from about 8 to 10 $\mu g m^{-3}$. ATOLL, Creil

310

315



and Talence sites have higher PM₁ concentrations (between 10 and 10.4 μg m⁻³): the first two (located in the northern Hauts-de-France region) are influenced by higher NO₃ concentration levels of 3.1 and 2.4 μg m⁻³, respectively, whereas Talence (near Bordeaux in the southern Nouvelle-Aquitaine region) has a strong contribution of OA (6.0 μg m⁻³).

320 The high NO₃ levels at the two sites in northern France are attributed to road traffic and combustion emissions (rich in nitrogen oxides; NO_x), which combine with ammonia (NH₃), typically associated with agricultural activities, forming ammonium nitrate (NH₄NO₃; AN) under favorable meteorological conditions (Roig Rodelas et al., 2019), as well as to transboundary pollution from Eastern Europe (Chebaicheb et al., 2023). Conversely,

325 Talence has the highest 95th percentile of OA (higher than 19.0 μg m⁻³, Fig. 3), associated with strong biomass combustion in the Bordeaux area during the cold season (Favez et al., 2021).

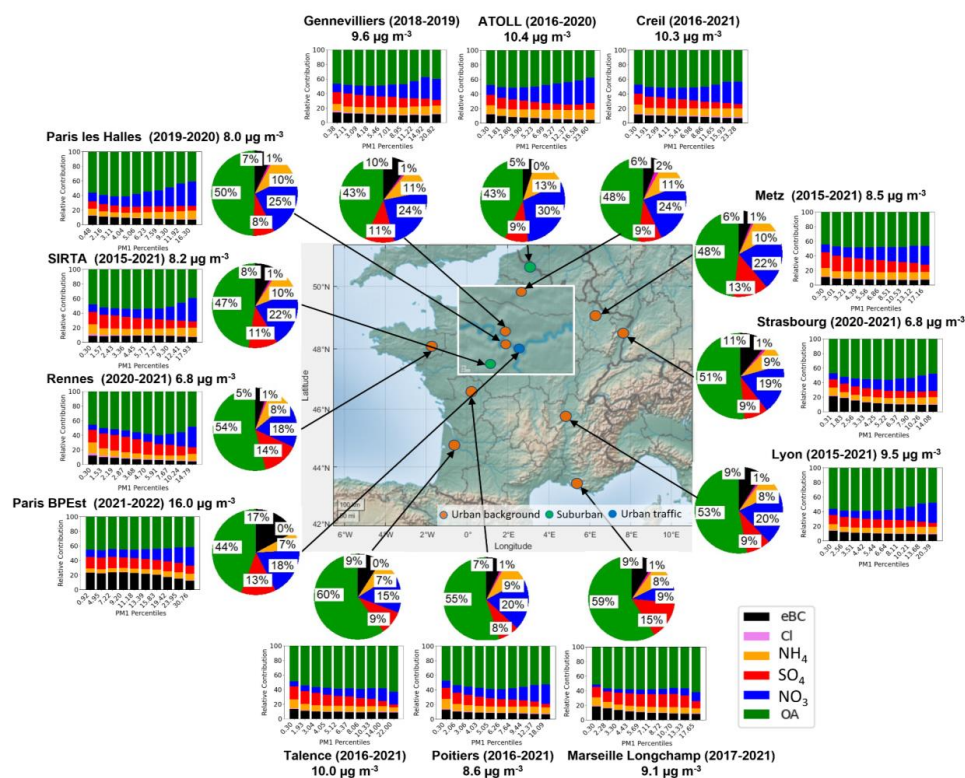


Figure 2: Multi-annual averaged PM₁ mass concentration and pie charts of average relative contributions of non-refractory species and eBC at different sites in France; the bar charts represent the relative contribution as a function of PM₁ deciles.

330

For the Greater Paris region, the SIRTA facility is located 22 and 25 km away from the sites representing central areas of Paris, i.e., Paris Les Halles and Gennevilliers, respectively. Logically, due to the closer proximity with intense emission sources, Gennevilliers exhibits higher PM₁ concentrations (9.6 μg m⁻³ on average over the 2018-2019 period) compared to SIRTA levels of 8.2 μg m⁻³. The comparable PM₁ loading presented here between Paris Les Halles (8.0 μg m⁻³) and SIRTA is probably linked to the specific measurement periods analyzed for each site.

335



340

Indeed, data from Paris Les Halles presented here include the COVID-19 lockdown periods of 2020–2021, while SIRTA data are averaged over 2015–2021. When averaged over the same period as Paris Les Halles, the PM_{10} level at SIRTA decreases to $6.2 \mu g m^{-3}$. Moreover, an increased mixing layer height over the Paris city center, due to the urban heat island effect which may dilute the aerosol content in a wider volume, should also be considered when comparing concentrations from inner and suburban sites within such a megapolis (e.g., Dupont et al., 2016).

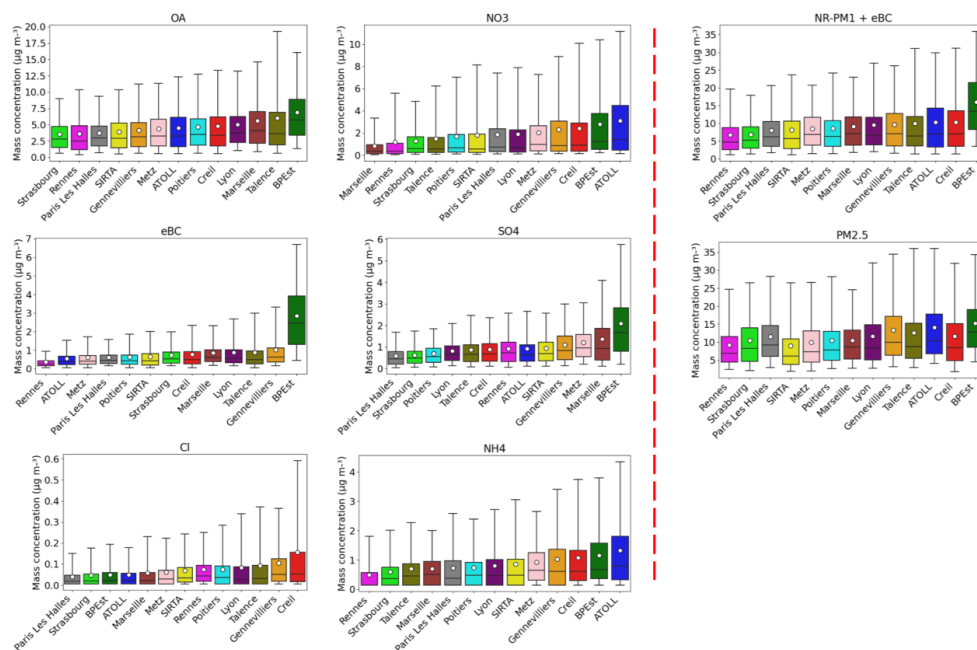


Figure 3: Box plots of the statistical distribution (5th, 25th, 50th, 75th and 95th percentiles) of each NR- PM_{10} species and eBC, as well as PM_{10} and $PM_{2.5}$ mass concentrations; means are indicated by the circle symbol.

345

The analysis of individual contributions shows that organic compounds make up about half of the PM_{10} total mass across all sites, ranging from 43 to 60 %, which is comparable with the average of OA at urban sites in Europe (around 50 % of PM_{10}), as reported by Chen et al., (2022). It is also consistent with the OA relative contribution observed by Bressi et al., (2021) in Europe (36–64 % of NR- PM_{10}). The stations located in central and southern France, including Marseille-Longchamp, Poitiers, Talence, and Lyon, show higher OA mass concentrations than sites in the north, which can be partly due to more intense secondary formation. Conversely, NO_3 contributions are more pronounced at northern sites (22–30 % vs 9–20 %), due to more favorable conditions for particulate AN formation (e.g., Favez et al., 2007). Consequently, NO_3 mass concentrations in France decreased from north to south and from east to west, consistent with the findings by Favez et al., (2021). Furthermore, NO_3 constitutes the second most significant contributor, accounting for 15–30 % of PM_{10} mass, except for Marseille-Longchamp, where it is less than 10 % ($0.8 \mu g m^{-3}$). Other studies have also reported the predominance of NO_3 over SO_4 at many European sites (Bressi et al. 2021, Chen et al. 2022). As Marseille is characterized by high emissions from industry

350

355



and shipping activities, the Marseille-Longchamp site exhibits a higher contribution of SO₄ (15 %), making it the second major contributor to PM₁ at that site (Chazeau et al., 2021).

360 Overall, SO₄ is the third largest contributor in France, with contributions ranging from 8 to 14 %. Besides Marseille-Longchamp and the BPEst traffic site, significant SO₄ concentrations are also obtained for Metz and Gennevilliers (around 1 µg m⁻³ on average), probably reflecting their transport from SO₂-rich regions, given that local emissions are considered low or negligible. Furthermore, SO₄ is considered to be influenced by long-range transport from Central Europe, which is the case for many sites in northern and Eastern France, including SIRTA, ATOLL, Creil, Paris Les Halles, Strasbourg, and Poitiers.

365 For the remaining compounds, mean NH₄ levels range from 0.5 to 1.3 µg m⁻³, with a contribution fluctuating between 7 % and 13 %, showing a strong correlation with NO₃ and SO₄ levels, linked to the neutralization of sulfuric and nitric acids by NH₃. Meanwhile, the contribution of eBC varies from 5 to 11 % at the urban background sites investigated here. Previous studies, including Chen et al. (2022), reported higher contributions of BC at different European urban sites (12 %), which can be explained by recent changes in data processing, as discussed
370 in Section 2.3.2. Finally, Cl makes a minor contribution of around 1 % at all sites, with averaged mass concentrations generally very low, remaining below 0.1 µg m⁻³, except for Gennevilliers (0.1 µg m⁻³) and Creil (0.15 µg m⁻³), with a slightly higher contribution of 2 %. Ammonium chloride (AC; NH₄Cl) is formed in the atmosphere from the chemical reaction of hydrochloric acid (HCl) and NH₃. The main sources of HCl in the atmosphere are biomass combustion (Andreae et al., 1996), coal burning (Tobler et al., 2020, 2021), and waste combustion (McCulloch et al., 1999). In Creil, there is a large waste treatment plant 2 km northeast of the monitoring station, which could explain the higher concentration of Cl observed at this site (Fig. S3). Similarly, in
375 Gennevilliers, industrial emissions could explain occasional spikes measured during easterly winds.

Figure 2 also illustrates the variations in PM₁ chemical composition as a function of PM₁ mass concentrations, divided into 10 concentration levels (corresponding to deciles) for each site. OA exhibits even higher contributions
380 at high PM₁ mass concentrations at Talence, Marseille-Longchamp, and Poitiers especially during the coldest and warmest months of the year (Figure S4). This can generally be explained by the influence of biomass burning during winter pollution episodes as also previously described for the Paris area (Petit et al., 2015; Foret et al., 2022), and by the impact of secondary formation of organic compounds and emissions from forest fires in summer (Chen et al., 2022). However, OA decreases from the 30th percentile (around 4 to 5 µg m⁻³) of PM₁ levels with an
385 increase in NO₃ at sites in northern France and Lyon. NO₃ plays an important role during pollution events, particularly in spring, as reported previously in France (Dupont et al., 2016; Petit et al., 2017; Zhang et al., 2020) and at other mid-latitude European sites (Bressi et al., 2021).

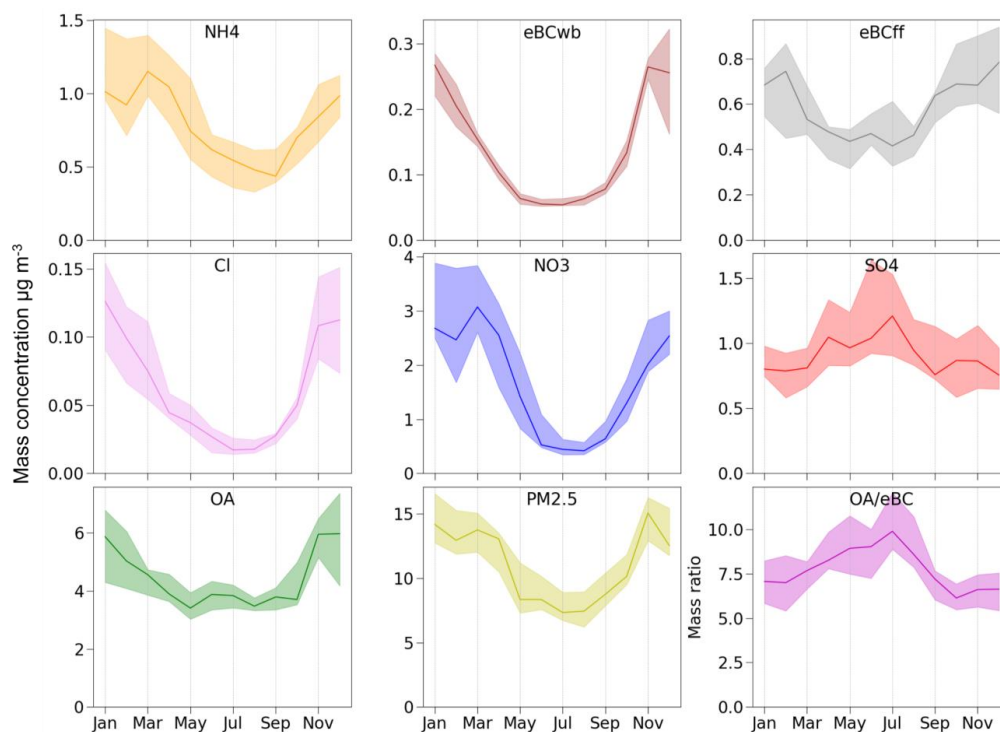
The contributions of SO₄ and eBC are generally stable or show a slight decrease with increasing PM₁. Nevertheless, eBC exhibits significant contributions at lower PM₁ levels at BPEst and, to a lesser extent, Marseille-Longchamp,
390 Strasbourg, and Rennes, indicating significant local combustion sources at those sites. Furthermore, Marseille-Longchamp exhibits fairly consistent OA, NO₃, and SO₄ contributions to PM₁ levels, showing nonetheless a significant increase of the first two during pollution events. Globally, SO₄ is a relevant contributor for Metz, Rennes, Gennevilliers, SIRTA, Talence, and Marseille-Longchamp, while OA retains significance at all sites throughout the PM₁ percentiles.



395 **3.2 Seasonal and diel cycles of fine aerosol chemical species**

The averaged seasonal and diel cycles were investigated for the different chemical species at all sites. Figure 4 shows the median and interquartile range (IQR) monthly variability for each species considered here, over the averaged cycles for the (sub)urban sites over France. The averaged monthly variabilities of the PM₁ species for each site are shown in Figure S5.

400 All chemical species exhibit significant variability in mass concentration over the months. In particular, eBC_{wb} shows a clear seasonality, with higher concentrations during winter (around an average of 0.3 µg m⁻³) compared to summer (0.05 µg m⁻³), as expected due to the high level of wood combustion for residential heating in wintertime. Furthermore, there is substantial variability between sites in winter (represented by a larger IQR), probably as a result of different meteorological conditions, as well as the fraction of wood combustion for residential heating in the surroundings. Conversely, eBC_{fr} shows seasonal variations comparable to eBC_{wb}, but with smaller winter/summer difference spans ranging from around 0.4 to 0.7 µg m⁻³ in May and October, respectively. This variability is associated with seasonal meteorological conditions favoring (or not) the accumulation of atmospheric pollutants, compounded to a lesser extent to changes in road traffic intensity, leading to a maximum commonly observed in autumn (Petit et al., 2015). Similarly, OA displays higher levels during cold seasons (5.5 µg m⁻³), with reasons comparable to those for eBC, and lower levels during warm periods (3.5 µg m⁻³). Nevertheless, OA peaks (with a higher OA/eBC mass ratio) in summer, reflecting the formation of SOA from biogenic and anthropogenic sources (Favez et al., 2007). Notably, SOAs are formed mainly from biogenic VOC in summer, when temperatures and sunlight are high (Canonaco et al., 2015; Cao et al., 2022), but also during nighttime, likely associated with nitrate chemistry (Kiendler-Scharr et al., 2016). Furthermore, OA yields lower site-to-site variability (i.e., IQR) (Fig. S6), as most of the OA, even in wintertime, is associated with regional processes and secondary formation (Chen et al., 2022; Chebaicheb et al., 2023).



420 **Figure 4: Monthly variability of mass concentrations of PM₁ species, PM_{2.5}, and OA/eBC ratio across all sites. The Figure shows the median and IQR (25th and 75th percentiles) calculated from the averaged monthly concentrations for each site. Months were considered only if data coverage was at least 75 %.**

NO₃ and NH₄ concentrations display a marked seasonal pattern, peaking in late winter and early spring, and averaging around 3.0 and 1.2 μg m⁻³, respectively. As discussed in the previous section, AN concentrations depend on site-specific factors, contributing to a greater variability between sites. In contrast, SO₄ shows a relatively stable monthly variation, with higher levels observed between April and August. Elevated summertime SO₄ concentrations could be attributed to favorable meteorological conditions. In addition, SO₄ can either be formed “locally” from the oxidation of SO₂ or transported from emission hotspots, such as Eastern European regions (Roig Rodelas et al., 2019). Cl exhibits a strong seasonality, ranging from 0.02 (summer) to 0.14 μg m⁻³ (winter). The higher concentrations of HCl during the cold seasons can be partly attributed to its semi-volatile nature (similarly to AN, its formation should be favored by low temperatures and high humidity), as well as transport from emission hotspots areas, notably of intense coal combustion, further enhanced during wintertime (Tobler et al., 2021).

The mean diel profiles obtained for each chemical species across all (sub)urban background sites and for each season are shown in Figure 5. All species exhibit higher concentrations at night, which could be, at least partially, associated with a lower boundary layer height. Some species show variability associated with local emission sources, including road traffic (morning and evening peaks), notably for OA and eBC_{ff}, with consistent behavior throughout the year. OA shows a stronger nighttime peak, notably during the colder months, mimicking eBC_{wb} associated with wood heating. OA enhancement during nighttime in wintertime is linked with residential heating



under a lower boundary layer (Chebaicheb et al., in prep.). Furthermore, at Paris Les Halles, in the heart of the city center, OA further exhibits a small peak at noon (Fig. S7), pointing to a possible influence of cooking emissions at this site. Overall, the $PM_{2.5}$ profile aligns with OA diel cycles, with higher loadings during the morning and evening hours, due to the predominance of the organic species in the fine aerosol fraction.

440

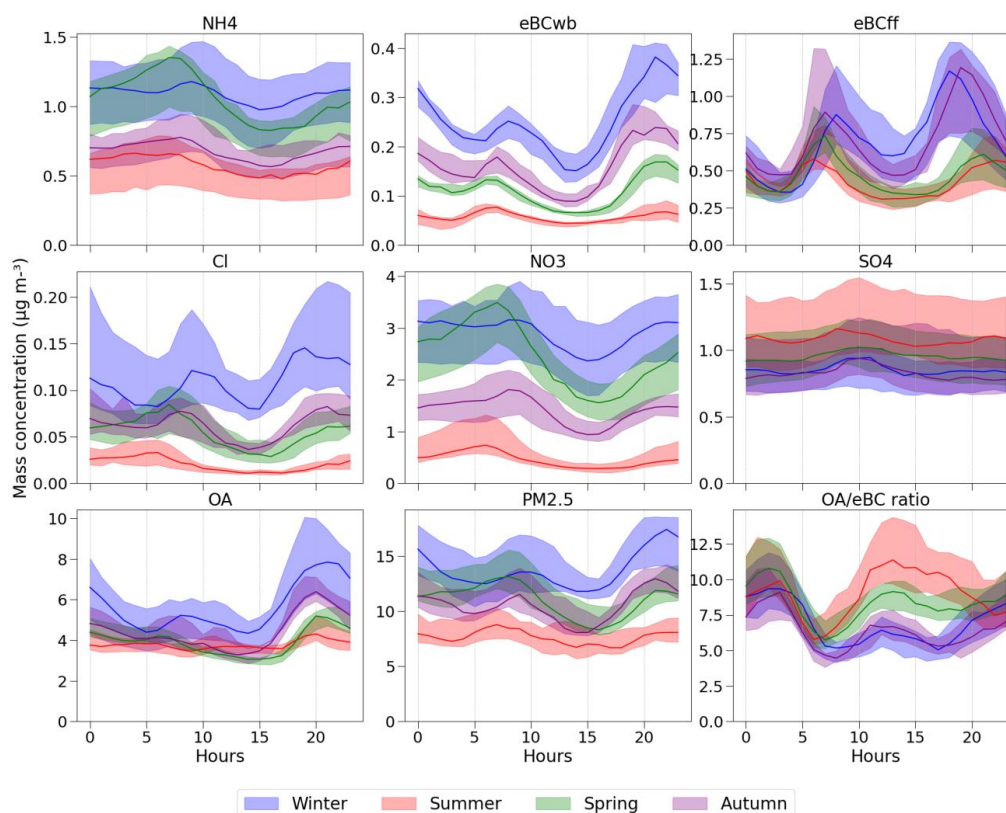


Figure 5: Seasonal median and IQR of daily profiles for all sites for each PM_1 component, $PM_{2.5}$, and OA/eBC ratio.

Both NO_3 and NH_4 display a comparable diel cycle, featuring higher mass concentrations during the morning hours in all seasons, albeit at different levels. Lower temperatures and higher relative humidity in the morning favor the formation of AN. During the day, as temperatures rise, AN concentrations decrease due to the evaporation into the gas phase of NH_3 and HNO_3 . Consequently, AN mass concentrations are lowest in summer, due to unfavorable weather conditions and, to some extent, reduced NO_x levels associated with the school holidays (Roig Rodelas et al., 2019). As discussed previously, AN levels are highest in spring, due to favorable meteorological conditions and intensive agricultural activities. On the other hand, the diel cycle of SO_4 shows relatively constant values during the day, with higher levels observed in summer, as discussed previously. Notably, the diel cycle of SO_4 at some sites features morning or afternoon peaks, especially for Lyon and Marseille-Longchamp sites, which may be explained by the presence of local (Chazeau et al., 2021) or regional sources (Fig. S7, S8, and S9).

445

450



455 Finally, the OA/eBC ratio shows an interesting diel cycle, exhibiting greater values at night in all seasons, ranging from 8 to 12, possibly associated with nighttime SOA formation or OA-rich sources such as wood combustion. This ratio also increases during the day, which could be explained by photochemistry and SOA formation, particularly of biogenic origin during summertime (Chebaicheb et al., 2023). As expected, the ratio decreases during the morning and evening rush hours, associated with more BC-rich traffic emissions.

3.3 Examples of comparison between our observations and chemical transport model outputs

460 In this section, CHIMERE model results for 2018, with a spatial resolution of 7 km over France, were used to compare with PM₁ observations. The simulation results could only be compared with 9 of the sites analyzed here. BPEst, Paris Les Halles, Rennes, and Strasbourg were excluded from this analysis because measurements at these sites only started after 2018. The time series of observed and modeled concentrations are shown in the supporting material (Figure S10). Figure 6 summarizes results from the comparison between observations and simulations, 465 typically showing good agreement. Loadings for inorganics (NO₃, SO₄, NH₄, and Cl) and eBC are fairly well-captured by the model across all sites, with some exceptions. In particular, at the Marseille-Longchamp site, SO₄, NO₃, NH₄, and eBC are consistently underestimated by the model (33, 41, 45, and 65 %, respectively). This discrepancy could be due to the low resolution of the model grid (7 km over France) that may not be sufficient to capture local meteorology or sources, or more broadly a potential underestimation of emissions in the Southeastern region of France. Several sites also present an underestimation of SO₄ (Metz, SIRTA, Talence) by around 35-39 470 %. In contrast, NO₃ is strongly overestimated by the model (57 %) in the north of France (ATOLL). Organics, on the other hand, are consistently underestimated by the model at all sites by a factor of 2-3. Other recent studies also reported underestimations of OA at 11 European sites, focusing on winter 2009 (Ciarelli et al., 2016). In the present study, OA yields a strong underestimation particularly in the warmer months (60 % vs. 41 % for the colder 475 months).

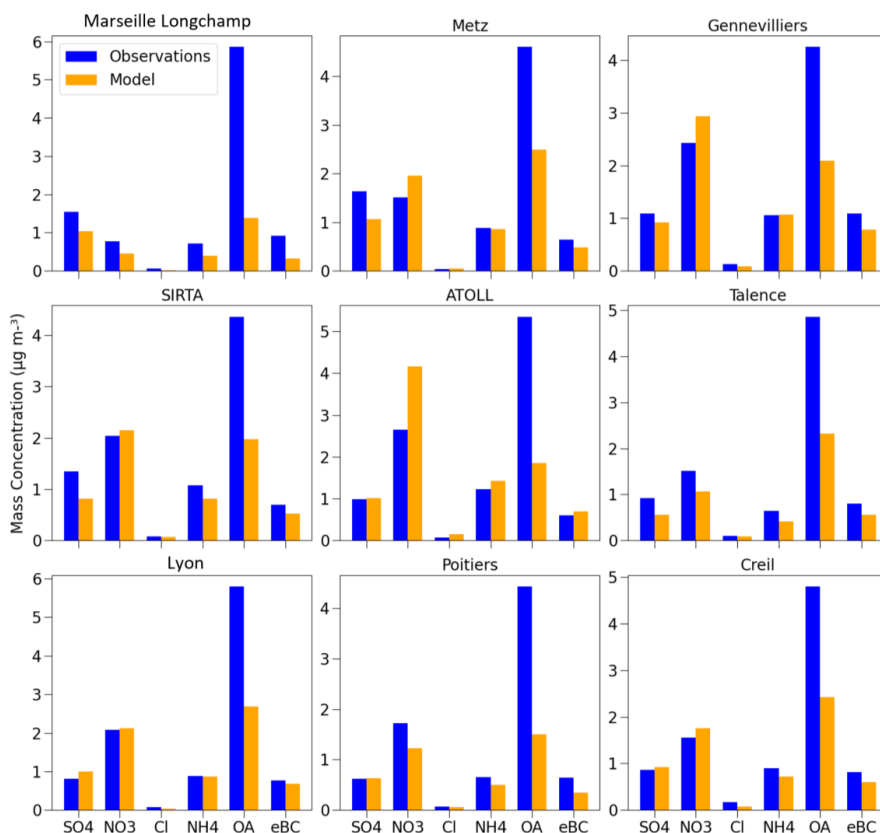


Figure 6: Mean mass concentration (in $\mu\text{g m}^{-3}$) of different chemical species for observations (in blue) and simulations (in orange) at nine French sites over the year 2018.

480 Figure 7 displays the diel profiles of each species, comparable with Figure 5, however restricted to the winter and summer of 2018, allowing the comparison with model outputs. In general, the species exhibit relatively consistent model performance between winter and summer, although there is an underestimation by the model for the latter. For NO_3 , the concentrations observed during wintertime are relatively stable throughout the day, whereas the model shows a strong daytime decrease due to the modeled evaporation of ammonium nitrate. During summertime, enhancement of NO_3 in the early morning is captured by both observations and model, however as a smooth nighttime increase/decrease for the former, and a sharp peak in the latter. A similar pattern is observed for NH_4 . For SO_4 , the diel profile is quite constant for both observations and simulations in summer. In winter, the slight increase of SO_4 during the day is not captured by the model, which instead shows a low peak at night. For eBC, both observations and model simulations show two peaks during rush hours. In winter, the night peak is more pronounced in the model, but nonetheless they display comparable levels, in contrast to summertime, when the model tends to underestimate the concentrations. These differences in daily eBC profiles may be attributed to meteorological conditions or issues in the seasonal temporality of emissions. Finally for OA, as discussed before, the model largely underestimates observations in summer. Generally, the behavior is fairly well represented, however wintertime nighttime enhancement is larger than observations, similar to eBC.

485

490



495 Figure 8 presents some statistical parameters (mean bias, normalized *Root Mean Square Error* (RMSE), and correlation coefficient r) calculated from the daily means for each chemical species across the nine urban sites in France. Overall, the correlations between observations and model results show good agreement, with correlation coefficients (r) ranging between 0.6 and 0.8, which is consistent with the literature (Couvidat et al., 2018, Cholakian et al. 2018). The mean bias and normalized RMSE confirm the model robustness. Mean bias is nearly negligible for SO_4 , NO_3 , NH_4 , Cl , and eBC, and approximately $-2 \mu\text{g m}^{-3}$ for OA, up to $-4 \mu\text{g m}^{-3}$ for the Marseille Longchamp site. RMSE exhibits a slightly more scattered distribution, generally ranging between 0.5 and $2 \mu\text{g m}^{-3}$.

500

3.

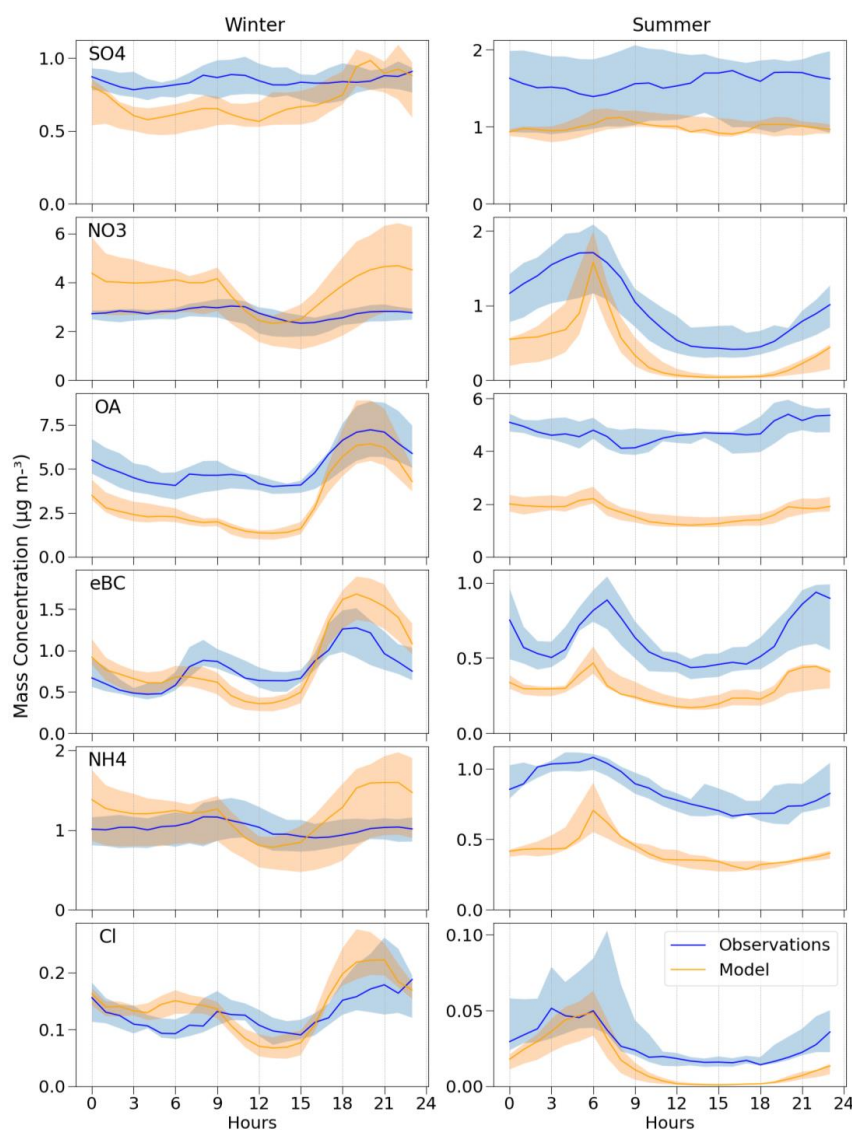
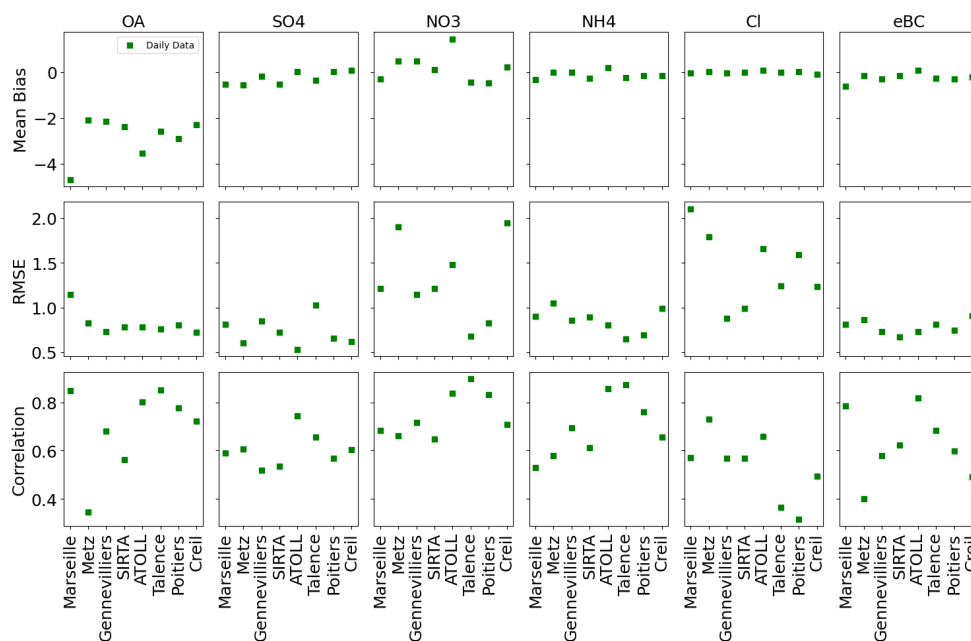


Figure 7: Observed and modeled diel profiles during the winter and summer of 2018 across 9 French sites.



505 **Figure 8: Statistic parameters (mean bias, normalized RMSE, and correlation coefficient r) for different species at each site, using daily averages.**

Furthermore, we could compare the model results with offline chemical information from filter samples collected in the submicron aerosol fraction at four sites in 2018. These filter samples were collected daily from March 15th to April 29th, 2018 in Talence, from February 16th to April 1st in Poitiers, from January 1st to January 23rd, from
 510 May 13th to May 27th, and from September 19th to September 22nd in Lyon, as well as every 4 hours from July 5th to July 27th in Marseille-Longchamp. They were analyzed in the laboratory for their organic carbon (OC), elemental carbon (EC), SO_4 , NO_3 , and NH_4 loadings. Figure S11 illustrates the comparison between model simulations and either online or offline observations, for these four sites with respect to OA, NO_3 , NH_4 , SO_4 , and eBC.

515 A higher correlation is observed between simulations and ACSM observations for OA, NO_3 , and NH_4 compared to filters (with r^2 values of 0.5, 0.7, and 0.6 with ACSM, as opposed to 0.24, 0.54, and 0.36 with filters, respectively). SO_4 and eBC show relatively similar correlations (with r^2 values of 0.44 and 0.42 with ACSM and AE33, respectively, and 0.18 and 0.11 with filters, respectively), but they exhibit different slopes (the model vs. ACSM-AE33 PM_1 demonstrates higher slopes at 0.45 and 0.5 compared to 0.36 and 0.33 with filters). Overall, the
 520 comparison of model results with observations from ACSM and AE33 shows higher correlations than with filter analyses, emphasizing the importance of online measurements for validating air quality models.

4 Conclusions

This study presents multiannual measurements of ACSM and AE33 collected at 13 (sub)urban sites that are part of the French CARA program. The datasets ranged from 1 to 6 years, between 2015 and 2021. Two of those sites



525 are integrated into the ACTRIS European infrastructure, namely ATOLL (near Lille) and SIRTA (near Paris). The dataset contains submicron aerosol species, OA, NO₃, NH₄, SO₄, Cl, and eBC, deconvolved into eBC_{ff} and eBC_{wb}. A meticulous process of quality control, technical validation, and environmental assessment was employed to validate homogeneously and rigorously the datasets. This process followed the guidelines provided by the French reference laboratory for air quality monitoring and adhered strictly to the ACTRIS standard operating procedures.

530 This article presents a comprehensive overview of these long-term datasets, offering an analysis of the geographical disparities in PM₁ chemical composition, as well as the main seasonal and diel variations in fine particle content.

Across all sites, OA is the predominant compound, with a mean concentration of 4.7 μg m⁻³ (43-60 %) in PM₁, followed by NO₃ (15-30 %), SO₄ (8-14 %), NH₄ (7-13 %), and eBC (5-11 %). Stations in central and southern France exhibit higher OA mass concentrations (5.3 μg m⁻³), likely attributed to more pronounced photochemical formation processes. Such secondary processes may also explain that OA is the predominant compound for the highest concentration levels in summertime at all sites. Additionally, for other seasons, OA exhibits greater contributions (>55 %) during periods of elevated PM₁ levels in the southern half of France, while NO₃ contributions (>40 %) are more notable during pollution episodes at northern sites, illustrating the competing influences on the aerosol chemical composition of biomass burning emissions and favorable meteorological conditions leading to the formation of ammonium nitrate, depending on the site location.

Temporal variations reveal distinct seasonality in PM₁ chemical species. eBC_{wb} and OA peak during wintertime, with values of around 0.3 and 5.5 μg m⁻³, respectively, typically associated with increased residential heating emissions. Those values peak particularly at night, combining stronger emissions and a potentially shallower boundary layer height, facilitating pollutant accumulation. OA also peaks in summer (3.5 μg m⁻³), typically associated with enhanced SOA formation. NO₃ peaks in late winter and early spring, correlated with a typical increase of NH₃ and favorable meteorological conditions during cold periods. Diel variations also exhibit unique characteristics at certain sites, such as the Paris Les Halles site, where an organic peak at noon suggests a significant contribution from cooking activities; similarly, a more pronounced rush hour enhancement at BPEst suggests a strong role of local traffic on OA levels.

Furthermore, the datasets presented here serve as essential tools for evaluating and validating regional and global air quality models. An illustrative comparison with CHIMERE is presented in this paper for 2018, encompassing nine French sites. Generally, the model successfully simulates inorganics (NO₃, SO₄, NH₄) and eBC but underestimates OA by 46-76 %, although with a high correlation between simulations and measurements (r between 0.6 and 0.8). Notably, NO₃ seems to be overestimated at the ATOLL site in northern France (57 %), whereas it is substantially underestimated by 29-42 % at southern sites. Overall, these multi-year datasets from French urban background sites hold significant value for the scientific community, enabling future research endeavors, including source apportionment studies, trend analyses, and epidemiological and health-related investigations.



560 **Data availability**

ACSM and AE33 datasets for SIRTAs and ATOLL (Villeneuve d'Ascq) are available in the EBAS database (<https://ebas.nilu.no/>). Other measurements are available on this open link (<https://zenodo.org/records/10790143>) (Chebaicheb et al., 2024).

Author contributions

| | |
|---|--|
| Data curation & Formal analysis | Mérodie Chatain, Benjamin Chazeau, Hasna Chebaicheb, Jean-Eudes Petit, Shouwen Zhang |
| Funding acquisition | Olivier Favez, Véronique Riffault |
| Investigation | Hasna Chebaicheb |
| Methodology | Hasna Chebaicheb |
| Resources | Gregory Abbou, Alexia Baudic, Mérodie Chatain, Benjamin Chazeau, Florian Couvidat, Raphaële Falhun, Florie Francony, Gregory Gille, Didier Grenier, Nicolas Marchand, Jean-Eudes Petit, Cyril Ratier, Véronique Riffault, Romain Vidaud, Shouwen Zhang |
| Supervision | Joel F. de Brito, Olivier Favez, Véronique Riffault |
| Validation | Joel F. de Brito, Olivier Favez, Véronique Riffault |
| Visualization | Hasna Chebaicheb |
| Writing – original draft preparation | Hasna Chebaicheb, Olivier Favez |
| Writing – review & editing | All co-authors |

565 **Funding**

This work was notably supported by the French Ministry of Environment, through direct funding of activities achieved by the AASQAs and the LCSQA in the frame of the CARA program. SIRTAs observations have been partly funded by the H2020 ACTRIS-2 project under grant agreement No 654109 as well as in the frame of the CNRS-INSU long-term monitoring aerosol program SNO CLAP as a component of the ACTRIS French Research

570 Instructure. Measurements conducted at ATOLL are also part of the Labex CaPPA project (ANR-11-LABX-0005-01), and the CLIMIBIO and ECRIN projects, both also funded by the Regional Council “Hauts-de-France” and the European Regional Development Fund (ERDF). Observations at the Marseille Longchamp supersite benefited from complementary financial support from the PACA region (PRISM project; grant n° 2017_08809).

Acknowledgments

575 The authors are deeply grateful to many technicians, engineers, and scientists working in the AASQAs as well as at Ineris, IMT Nord Europe, LSCE, and LCE for their past and current involvement in the long-term operation of the monitors and data handling at the sites investigated in the present study. Authors cannot cite each of them exhaustively but strongly hope they will all recognize themselves here.

Conflicts of Interest. The authors declare no conflict of interest.



580 References

- Allan, J. D., Delia, A. E., Coe, H., Bower, K. N., Alfarra, M. R., Jimenez, J. L., Middlebrook, A. M., Drewnick, F., Onasch, T. B., Canagaratna, M. R., Jayne, J. T., and Worsnop, D. R.: A generalised method for the extraction of chemically resolved mass spectra from Aerodyne aerosol mass spectrometer data, *J. Aerosol Sci.*, 35, 909–922, <https://doi.org/10.1016/j.jaerosci.2004.02.007>, 2004.
- 585 Alastuey, A., Querol, X., García, M., Trechera, P., Savadkoobi, M., Karanasiou, A., Minguillón, M. C., Fiebig, M., Dallénbach, K. R., Salameh, T., Sauvage, S., and Petäjä, T.: Deliverable D1 (D1.1): Guidelines, datasets of non-regulated pollutants incl. metadata, methods, 2022.
- Bond, T. C., Doherty, S. J., Fahey, D. W., Forster, P. M., Berntsen, T., DeAngelo, B. J., Flanner, M. G., Ghan, S., Kärcher, B., Koch, D., Kinne, S., Kondo, Y., Quinn, P. K., Sarofim, M. C., Schultz, M. G., Schulz, M., Venkataraman, C., Zhang, H., Zhang, S., Bellouin, N., Guttikunda, S. K., Hopke, P. K., Jacobson, M. Z., Kaiser, 590 J. W., Klimont, Z., Lohmann, U., Schwarz, J. P., Shindell, D., Storelvmo, T., Warren, S. G., and Zender, C. S.: Bounding the role of black carbon in the climate system: A scientific assessment, *J. Geophys. Res. Atmospheres*, 118, 5380–5552, <https://doi.org/10.1002/jgrd.50171>, 2013.
- Bressi, M., Cavalli, F., Putaud, J. P., Fröhlich, R., Petit, J.-E., Aas, W., Äijälä, M., Alastuey, A., Allan, J. D., Aurela, M., Berico, M., Bougiatioti, A., Bukowiecki, N., Canonaco, F., Crenn, V., Dusanter, S., Ehn, M., Elsasser, M., Flentje, H., Graf, P., Green, D. C., Heikkinen, L., Hermann, H., Holzinger, R., Hueglin, C., Keernik, H., Kiendler-Scharr, A., Kubelová, L., Lunder, C., Maasikmets, M., Makeš, O., Malaguti, A., Mihalopoulos, N., Nicolas, J. B., O'Dowd, C., Ovadnevaite, J., Petralia, E., Poulain, L., Priestman, M., Riffault, V., Ripoll, A., Schlag, P., Schwarz, J., Sciare, J., Slowik, J., Sosedova, Y., Stavroulas, I., Teinmaa, E., Via, M., Vodička, P., 600 Williams, P. I., Wiedensohler, A., Young, D. E., Zhang, S., Favez, O., Minguillón, M. C., and Prevot, A. S. H.: A European aerosol phenomenology - 7: High-time resolution chemical characteristics of submicron particulate matter across Europe, *Atmospheric Environ.* X, 10, 100108, <https://doi.org/10.1016/j.aeaoa.2021.100108>, 2021.
- Canagaratna, M. r., Jayne, J. t., Jimenez, J. l., Allan, J. d., Alfarra, M. r., Zhang, Q., Onasch, T. b., Drewnick, F., Coe, H., Middlebrook, A., Delia, A., Williams, L. r., Trimborn, A. m., Northway, M. j., DeCarlo, P. f., Kolb, C. e., Davidovits, P., and Worsnop, D. r.: Chemical and microphysical characterization of ambient aerosols with the aerodyne aerosol mass spectrometer, *Mass Spectrom. Rev.*, 26, 185–222, <https://doi.org/10.1002/mas.20115>, 2007.
- 605 Canonaco, F., Slowik, J. G., Baltensperger, U., and Prévôt, A. S. H.: Seasonal differences in oxygenated organic aerosol composition: implications for emissions sources and factor analysis, *Atmospheric Chem. Phys.*, 15, 6993–7002, <https://doi.org/10.5194/acp-15-6993-2015>, 2015.
- 610 Chazeau, B., Temime-Roussel, B., Gille, G., Mesbah, B., D'Anna, B., Wortham, H., and Marchand, N.: Measurement report: Fourteen months of real-time characterisation of the submicronic aerosol and its atmospheric dynamics at the Marseille–Longchamp supersite, *Atmospheric Chem. Phys.*, 21, 7293–7319, <https://doi.org/10.5194/acp-21-7293-2021>, 2021.



- 615 Chazeau et al, Organic aerosol source apportionment by using rolling positive matrix factorization: Application to a Mediterranean coastal city, *Atmospheric environment: X*, 2022
- Chebaicheb, H., F. de Brito, J., Chen, G., Tison, E., Marchand, C., Prévôt, A. S. H., Favez, O., and Riffault, V.: Investigation of four-year chemical composition and organic aerosol sources of submicron particles at the ATOLL site in northern France, *Environ. Pollut.*, 330, 121805, <https://doi.org/10.1016/j.envpol.2023.121805>, 2023.
- 620 Chebaicheb, H et al., Phenomenology of organic aerosol multi-annual source apportionment at 12 urban and peri-urban sites in France, in preparation.
- Chebaicheb, H., Ferreira De Brito, J., Amodeo, T., Couvidat, F., Petit, J.-E., Tison, E., Abbou, G., Alexia, B., Chatain, M., Chazeau, B., Marchand, N., Falhun, R., Francony, F., Ratier, C., Grenier, D., Vidaud, R., Zhang, S., Gille, G., Meunier, L., Marchand, C., Riffault, V., and Favez, O.: Multi-year high time resolution measurements of fine PM at 13 sites of the French Operational Network (CARA program), <https://doi.org/10.5281/zenodo.10790143>, 2024.
- 625 Chen, G., Canonaco, F., Tobler, A., Aas, W., Alastuey, A., Allan, J., Atabakhsh, S., Aurela, M., Baltensperger, U., Bougiatioti, A., De Brito, J. F., Ceburnis, D., Chazeau, B., Chebaicheb, H., Daellenbach, K. R., Ehn, M., El Haddad, I., Eleftheriadis, K., Favez, O., Flentje, H., Font, A., Fossom, K., Freney, E., Gini, M., Green, D. C., Heikkinen, L., Herrmann, H., Kalogridis, A.-C., Keernik, H., Lhotka, R., Lin, C., Lunder, C., Maasikmets, M., Manousakas, M. I., Marchand, N., Marin, C., Marmureanu, L., Mihalopoulos, N., Močnik, G., Nęcki, J., O'Dowd, C., Ovadnevaite, J., Peter, T., Petit, J.-E., Pikridas, M., Matthew Platt, S., Pokorná, P., Poulain, L., Priestman, M., Riffault, V., Rinaldi, M., Róžański, K., Schwarz, J., Sciare, J., Simon, L., Skiba, A., Slowik, J. G., Sosedova, Y., Stavroulas, I., Styszko, K., Teinmaa, E., Timonen, H., Tremper, A., Vasilescu, J., Via, M., Vodička, P., Wiedensohler, A., Zografou, O., Cruz Minguillón, M., and Prévôt, A. S. H.: European aerosol phenomenology – 8: Harmonised source apportionment of organic aerosol using 22 Year-long ACSM/AMS datasets, *Environ. Int.*, 166, 107325, <https://doi.org/10.1016/j.envint.2022.107325>, 2022.
- 635 Campagne 2021 d'étalonnage et de comparaison inter-laboratoire (CIL) des Q-ACSM | LCSQA: <https://www.lcsqa.org/fr/rapport/campagne-2021-detallonnage-et-de-comparaison-inter-laboratoire-cil-des-q-acsm>, last access: 24 October 2023.
- 640 Cholakian, A., Beekmann, M., Colette, A., Coll, I., Siour, G., Sciare, J., Marchand, N., Couvidat, F., Pey, J., Gros, V., Sauvage, S., Michoud, V., Sellegri, K., Colomb, A., Sartelet, K., Langley DeWitt, H., Elser, M., Prévôt, A. S. H., Szidat, S., and Dulac, F.: Simulation of fine organic aerosols in the western Mediterranean area during the ChArMEx 2013 summer campaign, *Atmospheric Chem. Phys.*, 18, 7287–7312, <https://doi.org/10.5194/acp-18-7287-2018>, 2018.
- 645 Chrit, M., Sartelet, K., Sciare, J., Pey, J., Marchand, N., Couvidat, F., Sellegri, K., and Beekmann, M.: Modelling organic aerosol concentrations and properties during ChArMEx summer campaigns of 2012 and 2013 in the western Mediterranean region, *Atmospheric Chem. Phys.*, 17, 12509–12531, <https://doi.org/10.5194/acp-17-12509-2017>, 2017.



- 650 Ciarelli, G., Aksoyoglu, S., Crippa, M., Jimenez, J.-L., Nemitz, E., Sellegri, K., Äijälä, M., Carbone, S., Mohr, C., O'Dowd, C., Poulain, L., Baltensperger, U., and Prévôt, A. S. H.: Evaluation of European air quality modelled by CAMx including the volatility basis set scheme, *Atmospheric Chem. Phys.*, 16, 10313–10332, <https://doi.org/10.5194/acp-16-10313-2016>, 2016.
- Couvidat, F. and Sartelet, K.: The Secondary Organic Aerosol Processor (SOAP v1.0) model: a unified model with different ranges of complexity based on the molecular surrogate approach, *Geosci. Model Dev.*, 8, 1111–1138, <https://doi.org/10.5194/gmd-8-1111-2015>, 2015.
- Couvidat, Florian, et Bertrand Bessagnet. 2021. « Role of ecosystem-atmosphere exchanges of semi-volatile organic compounds in organic aerosol formation ». *Atmospheric Environment* 263 (octobre): 118541. <https://doi.org/10.1016/j.atmosenv.2021.118541>.
- 660 Couvidat, Florian, Bertrand Bessagnet, Marta Garcia-Vivanco, Elsa Real, Laurent Menut, et Augustin Colette. 2018. « Development of an Inorganic and Organic Aerosol Model (CHIMERE 2017β v1.0): Seasonal and Spatial Evaluation over Europe ». *Geoscientific Model Development* 11 (1): 165-94. <https://doi.org/10.5194/gmd-11-165-2018>.
- Crenn, V., Fronval, I., Petitprez, D., Riffault, V., 2017. Fine particles sampled at an urban background site and an industrialized coastal site in Northern France — Part I: Seasonal variations and chemical characterization. *Sci. Total Environ.* 578, 203–218. <https://doi.org/10.1016/j.scitotenv.2015.11.165>
- 665 Daellenbach, K. R., Bozzetti, C., Křepelová, A., Canonaco, F., Wolf, R., Zotter, P., Fermo, P., Crippa, M., Slowik, J. G., Sosedova, Y., Zhang, Y., Huang, R.-J., Poulain, L., Szidat, S., Baltensperger, U., El Haddad, I., and Prévôt, A. S. H.: Characterization and source apportionment of organic aerosol using offline aerosol mass spectrometry, *Atmospheric Meas. Tech.*, 9, 23–39, <https://doi.org/10.5194/amt-9-23-2016>, 2016.
- 670 Drinovec, L., Močnik, G., Zotter, P., Prévôt, A. S. H., Ruckstuhl, C., Coz, E., Rupakheti, M., Sciare, J., Müller, T., Wiedensohler, A., and Hansen, A. D. A.: The “dual-spot” Aethalometer: an improved measurement of aerosol black carbon with real-time loading compensation, *Atmospheric Meas. Tech.*, 8, 1965–1979, <https://doi.org/10.5194/amt-8-1965-2015>, 2015.
- 675 Dupont, J.-C., Haefelin, M., Badosa, J., Elias, T., Favez, O., Petit, J. E., Meleux, F., Sciare, J., Crenn, V., and Bonne, J. L.: Role of the boundary layer dynamics effects on an extreme air pollution event in Paris, *Atmos. Environ.*, 141, 571–579, <https://doi.org/10.1016/j.atmosenv.2016.06.061>, 2016.
- European Environment Agency, 2023. Harm to human health from air pollution in Europe: burden of disease 2023. <https://www.eea.europa.eu/publications/harm-to-human-health-from-air-pollution> (accessed 3.4.24).
- 680 Favez, O., Cachier, H., Sciare, J., and Le Moullec, Y.: Characterization and contribution to PM_{2.5} of semi-volatile aerosols in Paris (France), *Atmos. Environ.*, 41, 7969–7976, <https://doi.org/10.1016/j.atmosenv.2007.09.031>, 2007.



- 685 Favez, O., El Haddad, I., Piot, C., Boréave, A., Abidi, E., Marchand, N., Jaffrezo, J.-L., Besombes, J.-L., Personnaz, M.-B., Sciare, J., Wortham, H., George, C., and D'Anna, B.: Inter-comparison of source apportionment models for the estimation of wood burning aerosols during wintertime in an Alpine city (Grenoble, France), *Atmospheric Chem. Phys.*, 10, 5295–5314, <https://doi.org/10.5194/acp-10-5295-2010>, 2010.
- 690 Favez, O., Weber, S., Petit, J.-E., Alleman, L., Albinet, A., Riffault, V., Chazeau, B., Amodeo, T., Salameh, D., Zhang, Y., Srivastava, D., Samaké, A., Aujay, R., Papin, A., Bonnaire, N., Boullanger, C., Chatain, M., Chevrier, F., Detournay, A., and Leoz-Garziandia, E.: Overview of the French Operational Network for In Situ Observation of PM Chemical Composition and Sources in Urban Environments (CARA Program), <https://doi.org/10.20944/preprints202101.0182.v1>, 2021.
- Flentje, H., Mattis, I., Kipling, Z., Rémy, S., and Thomas, W.: Evaluation of ECMWF IFS-AER (CAMS) operational forecasts during cycle 41r1–46r1 with calibrated ceilometer profiles over Germany, *Geosci. Model Dev.*, 14, 1721–1751, <https://doi.org/10.5194/gmd-14-1721-2021>, 2021.
- 695 Foret, G., Michoud, V., Kotthaus, S., Petit, J.-E., Baudic, A., Siour, G., Kim, Y., Doussin, J.-F., Dupont, J.-C., Formenti, P., Gaimoz, C., Ghersi, V., Gratien, A., Gros, V., Jaffrezo, J.-L., Haeffelin, M., Kreitz, M., Ravetta, F., Sartelet, K., Simon, L., Té, Y., Uzu, G., Zhang, S., Favez, O., and Beekmann, M.: The December 2016 extreme weather and particulate matter pollution episode in the Paris region (France), *Atmos. Environ.*, 291, 119386, <https://doi.org/10.1016/j.atmosenv.2022.119386>, 2022.
- 700 Fortems-Cheiney, A., Dufour, G., Hamaoui-Laguel, L., Foret, G., Siour, G., Van Damme, M., Meleux, F., Coheur, P.-F., Clerbaux, C., Clarisse, L., Favez, O., Wallasch, M., and Beekmann, M.: Unaccounted variability in NH₃ agricultural sources detected by IASI contributing to European spring haze episode, *Geophys. Res. Lett.*, 43, 5475–5482, <https://doi.org/10.1002/2016GL069361>, 2016.
- 705 Freney, E., Zhang, Y., Croteau, P., Amodeo, T., Williams, L., Truong, F., Petit, J.-E., Sciare, J., Sarda-Esteve, R., Bonnaire, N., Arumae, T., Aurela, M., Bougiatioti, A., Mihalopoulos, N., Coz, E., Artinano, B., Crenn, V., Elste, T., Heikkinen, L., Poulain, L., Wiedensohler, A., Herrmann, H., Priestman, M., Alastuey, A., Stavroulas, I., Tobler, A., Vasilescu, J., Zanca, N., Canagaratna, M., Carbone, C., Flentje, H., Green, D., Maasikmets, M., Marmureanu, L., Minguillon, M. C., Prevot, A. S. H., Gros, V., Jayne, J., and Favez, O.: The second ACTRIS inter-comparison (2016) for Aerosol Chemical Speciation Monitors (ACSM): Calibration protocols and instrument performance evaluations, *Aerosol Sci. Technol.*, 53, 830–842, <https://doi.org/10.1080/02786826.2019.1608901>, 2019.
- 710 Fuzzi, S., Baltensperger, U., Carslaw, K., Decesari, S., Denier van der Gon, H., Facchini, M. C., Fowler, D., Koren, I., Langford, B., Lohmann, U., Nemitz, E., Pandis, S., Riipinen, I., Rudich, Y., Schaap, M., Slowik, J. G., Spracklen, D. V., Vignati, E., Wild, M., Williams, M., and Gilardoni, S.: Particulate matter, air quality and climate: lessons learned and future needs, *Atmospheric Chem. Phys.*, 15, 8217–8299, <https://doi.org/10.5194/acp-15-8217-2015>, 2015.
- Heikkinen, L., Äijälä, M., Daellenbach, K. R., Chen, G., Garmash, O., Aliaga, D., Graeffe, F., Rätty, M., Luoma, K., Aalto, P., Kulmala, M., Petäjä, T., Worsnop, D., and Ehn, M.: Eight years of sub-micrometre organic aerosol



- composition data from the boreal forest characterized using a machine-learning approach, *Atmospheric Chem. Phys.*, 21, 10081–10109, <https://doi.org/10.5194/acp-21-10081-2021>, 2021.
- 720 Jacobson, M. Z.: Strong radiative heating due to the mixing state of black carbon in atmospheric aerosols, *Nature*, 409, 695–697, <https://doi.org/10.1038/35055518>, 2001.
- Janssen, N. A. H., Hoek, G., Simic, -Lawson Milena, Fischer, P., van, B. L., ten, B. H., Keuken, M., Atkinson, R. W., Anderson, H. R., Brunekreef, B., and Cassee, F. R.: Black Carbon as an Additional Indicator of the Adverse Health Effects of Airborne Particles Compared with PM10 and PM2.5, *Environ. Health Perspect.*, 119, 1691–1699, <https://doi.org/10.1289/ehp.1003369>, 2011.
- 725 Kiendler-Scharr, A., Mensah, A.A., Friese, E., Topping, D., Nemitz, E., Prevot, A.S.H., Äijälä, M., Allan, J., Canonaco, F., Canagaratna, M., Carbone, S., Crippa, M., Dall'Osto, M., Day, D.A., De Carlo, P., Di Marco, C.F., Elbern, H., Eriksson, A., Freney, E., Hao, L., Herrmann, H., Hildebrandt, L., Hillamo, R., Jimenez, J.L., Laaksonen, A., McFiggans, G., Mohr, C., O'Dowd, C., Otjes, R., Ovadnevaite, J., Pandis, S.N., Poulain, L., Schlag, P., Sellegri, K., Swietlicki, E., Tiitta, P., Vermeulen, A., Wahner, A., Worsnop, D., Wu, H.-C., 2016. Ubiquity of organic nitrates from nighttime chemistry in the European submicron aerosol. *Geophys. Res. Lett.* 43, 7735–7744. <https://doi.org/10.1002/2016GL069239>
- Kuenen, J., Dellaert, S., Visschedijk, A., Jalkanen, J.-P., Super, I., and Denier van der Gon, H.: CAMS-REG-v4: a state-of-the-art high-resolution European emission inventory for air quality modelling, *Earth Syst. Sci. Data*, 14, 491–515, <https://doi.org/10.5194/essd-14-491-2022>, 2022.
- 735 P. Laj, C. L. Myhre, V. Riffault, V. Amiridis, H. Fuchs, K. Eleftheriadis, T. Petäjä, N. Kivekäs, E. Juurola, G. Saponaro, S. Philippin, C. Cornacchia, L. Alados Arboledas, H. Baars, A. Claude, M. De Mazière, B. Dils, L. Eder Murberg, M. Fiebig, M. Haefelin, H. Herrmann, K. Höhler, N. Illmann, A. Kreuter, E. Ludewig, E. Marinou, O. Möhler, L. Mona, D. Nicolae, E. O'Connor, R. M. Petracca Altieri, B. Picquet-Varrault, B. Popsichal, J.-P. Putaud, S. Reimann, T. Salameh, N. Siomos, I. Stachlewska, D. Van Pinxteren, K. A. Voudouri, U. Wandiger, A. Wiedensohler, A. Apituley, A. Comeron, M. Gysel-Beer, N. Mihalopoulos, N. Nikolova, A. Pietruczuk, S. Sauvage, J. Sciare, H. Skov, T. Svendby, E. Swietlicki, D. Toney, G. Vaughan, V. Zdimal, U. Baltensperger, J.-F. Doussin, M. Kulmala, G. Pappalardo, S. Sorvari Sundet, M. Vana, Aerosol, Cloud and Trace Gases Research Infrastructure - ACTRIS, the European research infrastructure supporting atmospheric science, in revision for
- 745 *Bulletin of the American Meteorological Society*.
- Lanz, V. A., Prévôt, A. S. H., Alfarra, M. R., Weimer, S., Mohr, C., DeCarlo, P. F., Gianini, M. F. D., Hueglin, C., Schneider, J., Favez, O., D'Anna, B., George, C., and Baltensperger, U.: Characterization of aerosol chemical composition with aerosol mass spectrometry in Central Europe: an overview, *Atmospheric Chem. Phys.*, 10, 10453–10471, <https://doi.org/10.5194/acp-10-10453-2010>, 2010.
- 750 LCSQA: Guide méthodologique pour la mesure du « Black Carbon » par Aethalomètre multi longueur d'onde AE33 dans l'air ambiant (Version 2020), 2020.
- LCSQA: CAHIER DES CHARGES POUR L'ETALONNAGE DES Q-ACSM, 2022.



- 755 Menut, L., Bessagnet, B., Briant, R., Cholakian, A., Couvidat, F., Mailler, S., Pennel, R., Siour, G., Tuccella, P., Turquety, S., and Valari, M.: The CHIMERE v2020r1 online chemistry-transport model, *Geosci. Model Dev.*, 14, 6781–6811, <https://doi.org/10.5194/gmd-14-6781-2021>, 2021.
- Middlebrook, A. M., Bahreini, R., Jimenez, J. L., and Cana-Garatna, M. R.: Evaluation of Composition-Dependent Collection Efficiencies for the Aerodyne Aerosol Mass Spectrometer using Field Data, *Aerosol Sci Technol*, 46, 258–271, 2011.
- 760 Ng, N. L., Herndon, S. C., Trimborn, A., Canagaratna, M. R., Croteau, P. L., Onasch, T. B., Sueper, D., Worsnop, D. R., Zhang, Q., Sun, Y. L., and Jayne, J. T.: An Aerosol Chemical Speciation Monitor (ACSM) for Routine Monitoring of the Composition and Mass Concentrations of Ambient Aerosol, *Aerosol Sci. Technol.*, 45, 780–794, <https://doi.org/10.1080/02786826.2011.560211>, 2011a.
- 765 Ng, N. L., Canagaratna, M. R., Jimenez, J. L., Zhang, Q., Ulbrich, I. M., and Worsnop, D. R.: Real-Time Methods for Estimating Organic Component Mass Concentrations from Aerosol Mass Spectrometer Data, *Environ. Sci. Technol.*, 45, 910–916, <https://doi.org/10.1021/es102951k>, 2011b.
- Petit, J.-E., Favez, O., Sciare, J., Crenn, V., Sarda-Estève, R., Bonnaire, N., Močnik, G., Dupont, J.-C., Haefelin, M., and Leoz-Garziandia, E.: Two years of near real-time chemical composition of submicron aerosols in the region of Paris using an Aerosol Chemical Speciation Monitor (ACSM) and a multi-wavelength Aethalometer, *Atmospheric Chem. Phys.*, 15, 2985–3005, <https://doi.org/10.5194/acp-15-2985-2015>, 2015.
- 770 Petit, J.-E., Amodeo, T., Meleux, F., Bessagnet, B., Menut, L., Grenier, D., Pellan, Y., Ockler, A., Rocq, B., Gros, V., Sciare, J., and Favez, O.: Characterising an intense PM pollution episode in March 2015 in France from multi-site approach and near real time data: Climatology, variabilities, geographical origins and model evaluation, *Atmos. Environ.*, 155, 68–84, <https://doi.org/10.1016/j.atmosenv.2017.02.012>, 2017.
- 775 Putaud, J.-P., Raes, F., Van Dingenen, R., Brüggemann, E., Facchini, M.-C., Decesari, S., Fuzzi, S., Gehrig, R., Hüglin, C., Laj, P., Lorbeer, G., Maenhaut, W., Mihalopoulos, N., Müller, K., Querol, X., Rodriguez, S., Schneider, J., Spindler, G., Brink, H. ten, Tørseth, K., and Wiedensohler, A.: A European aerosol phenomenology—2: chemical characteristics of particulate matter at kerbside, urban, rural and background sites in Europe, *Atmos. Environ.*, 38, 2579–2595, <https://doi.org/10.1016/j.atmosenv.2004.01.041>, 2004.
- 780 Roig Rodelas, R., Perdrix, E., Herbin, B., and Riffault, V.: Characterization and variability of inorganic aerosols and their gaseous precursors at a suburban site in northern France over one year (2015–2016), *Atmos. Environ.*, 200, 142–157, <https://doi.org/10.1016/j.atmosenv.2018.11.041>, 2019.
- Roig Rodelas, R., Chakraborty, A., Perdrix, E., Tison, E., Riffault, V., 2019. Real-time assessment of wintertime organic aerosol characteristics and sources at a suburban site in northern France. *Atmos. Environ.* 203, 48–61. <https://doi.org/10.1016/j.atmosenv.2019.01.035>
- 785 Roldin, P., Ehn, M., Kurtén, T., Olenius, T., Rissanen, M. P., Sarnela, N., Elm, J., Rantala, P., Hao, L., Hyttinen, N., Heikkinen, L., Worsnop, D. R., Pichelstorfer, L., Xavier, C., Clusius, P., Öström, E., Petäjä, T., Kulmala, M.,



- Vehkamäki, H., Virtanen, A., Riipinen, I., and Boy, M.: The role of highly oxygenated organic molecules in the Boreal aerosol-cloud-climate system, *Nat. Commun.*, 10, 4370, <https://doi.org/10.1038/s41467-019-12338-8>, 2019.
- 790 Sandradewi, J., Prévôt, A. S. H., Szidat, S., Perron, N., Alfarra, M. R., Lanz, V. A., Weingartner, E., and Baltensperger, U.: Using Aerosol Light Absorption Measurements for the Quantitative Determination of Wood Burning and Traffic Emission Contributions to Particulate Matter, *Environ. Sci. Technol.*, 42, 3316–3323, <https://doi.org/10.1021/es702253m>, 2008.
- Sartelet, K., Couvidat, F., Wang, Z., Flageul, C., and Kim, Y.: SSH-Aerosol v1.1: A Modular Box Model to Simulate the Evolution of Primary and Secondary Aerosols, *Atmosphere*, 11, 525, <https://doi.org/10.3390/atmos11050525>, 2020.
- 795 Saunders, S. M., Jenkin, M. E., Derwent, R. G., and Pilling, M. J.: Protocol for the development of the Master Chemical Mechanism, MCM v3 (Part A): tropospheric degradation of non-aromatic volatile organic compounds, *Atmospheric Chem. Phys.*, 3, 161–180, <https://doi.org/10.5194/acp-3-161-2003>, 2003.
- 800 Savadkoobi, M., Pandolfi, M., Reche, C., Niemi, J. V., Mooibroek, D., Titos, G., Green, D. C., Tremper, A. H., Hueglin, C., Liakakou, E., Mihalopoulos, N., Stavroulas, I., Artiñano, B., Coz, E., Alados-Arboledas, L., Beddows, D., Riffault, V., De Brito, J. F., Bastian, S., Baudic, A., Colombi, C., Costabile, F., Chazeanu, B., Marchand, N., Gómez-Amo, J. L., Estellés, V., Matos, V., van der Gaag, E., Gille, G., Luoma, K., Manninen, H. E., Norman, M., Silvergren, S., Petit, J.-E., Putaud, J.-P., Rattigan, O. V., Timonen, H., Tuch, T., Merkel, M., Weinhold, K.,
- 805 Vratolis, S., Vasilescu, J., Favez, O., Harrison, R. M., Laj, P., Wiedensohler, A., Hopke, P. K., Petäjä, T., Alastuey, A., and Querol, X.: The variability of mass concentrations and source apportionment analysis of equivalent black carbon across urban Europe, *Environ. Int.*, 178, 108081, <https://doi.org/10.1016/j.envint.2023.108081>, 2023.
- Schaap, M., Spindler, G., Schulz, M., Acker, K., Maenhaut, W., Berner, A., Wieprecht, W., Streit, N., Müller, K., Brüggemann, E., Chi, X., Putaud, J.-P., Hitznerberger, R., Puxbaum, H., Baltensperger, U., and ten Brink, H.: Artefacts in the sampling of nitrate studied in the “INTERCOMP” campaigns of EUROTRAC-AEROSOL, *Atmos. Environ.*, 38, 6487–6496, <https://doi.org/10.1016/j.atmosenv.2004.08.026>, 2004.
- 810 Sun, J., Zhang, Q., Canagaratna, M. R., Zhang, Y., Ng, N. L., Sun, Y., Jayne, J. T., Zhang, X., Zhang, X., and Worsnop, D. R.: Highly time- and size-resolved characterization of submicron aerosol particles in Beijing using an Aerodyne Aerosol Mass Spectrometer, *Atmos. Environ.*, 44, 131–140, <https://doi.org/10.1016/j.atmosenv.2009.03.020>, 2010.
- 815 Tobler, A. K., Skiba, A., Wang, D. S., Croteau, P., Styszko, K., Nęcki, J., Baltensperger, U., Slowik, J. G., and Prévôt, A. S. H.: Improved chloride quantification in quadrupole aerosol chemical speciation monitors (Q-ACSMs), *Atmospheric Meas. Tech.*, 13, 5293–5301, <https://doi.org/10.5194/amt-13-5293-2020>, 2020.
- Tobler, A. K., Skiba, A., Canonaco, F., Močnik, G., Rai, P., Chen, G., Bartyzel, J., Zimnoch, M., Styszko, K.,
- 820 Nęcki, J., Furger, M., Róžański, K., Baltensperger, U., Slowik, J. G., and Prevot, A. S. H.: Characterization of



- non-refractory (NR) PM₁ and source apportionment of organic aerosol in Kraków, Poland, *Atmospheric Chem. Phys.*, 21, 14893–14906, <https://doi.org/10.5194/acp-21-14893-2021>, 2021.
- 825 Viana, M., Kuhlbusch, T. A. J., Querol, X., Alastuey, A., Harrison, R. M., Hopke, P. K., Winiwarter, W., Vallius, M., Szidat, S., Prévôt, A. S. H., Hueglin, C., Bloemen, H., Wählin, P., Vecchi, R., Miranda, A. I., Kasper-Giebl, A., Maenhaut, W., and Hitzenberger, R.: Source apportionment of particulate matter in Europe: A review of methods and results, *J. Aerosol Sci.*, 39, 827–849, <https://doi.org/10.1016/j.jaerosci.2008.05.007>, 2008.
- Wang, Z., Couvidat, F., and Sartelet, K.: GENERator of reduced Organic Aerosol mechanism (GENOA v1.0): an automatic generation tool of semi-explicit mechanisms, *Geosci. Model Dev.*, 15, 8957–8982, <https://doi.org/10.5194/gmd-15-8957-2022>, 2022.
- 830 Wang, Z., Couvidat, F., and Sartelet, K.: Implementation of a parallel reduction algorithm in the GENERator of reduced Organic Aerosol mechanisms (GENOA v2.0): Application to multiple monoterpene aerosol precursors, *J. Aerosol Sci.*, 174, 106248, <https://doi.org/10.1016/j.jaerosci.2023.106248>, 2023.
- Wang, Z., Couvidat, F. and Sartelet, K. Response of biogenic secondary organic aerosol formation to anthropogenic NO_x emission mitigation. Submitted to *Science of The Total Environment*, 2024.
- 835 Watson, T. B.: Aerosol Chemical Speciation Monitor (ACSM) Instrument Handbook, <https://doi.org/10.2172/1375336>, 2017.
- Wittmaack, K. and Keck, L.: Thermodesorption of aerosol matter on multiple filters of different materials for a more detailed evaluation of sampling artifacts, *Atmos. Environ.*, 38, 5205–5215, <https://doi.org/10.1016/j.atmosenv.2004.05.047>, 2004.
- 840 WHO Air Quality Guidelines: https://www.c40knowledgehub.org/s/article/WHO-Air-Quality-Guidelines?language=en_US, last access: 23 January 2023.
- Zanatta, M., Gysel, M., Bukowiecki, N., Müller, T., Weingartner, E., Areskoug, H., Fiebig, M., Yttri, K. E., Mihalopoulos, N., Kouvarakis, G., Beddows, D., Harrison, R. M., Cavalli, F., Putaud, J. P., Spindler, G., Wiedensohler, A., Alastuey, A., Pandolfi, M., Sellegri, K., Swietlicki, E., Jaffrezo, J. L., Baltensperger, U., and Laj, P.: A European aerosol phenomenology-5: Climatology of black carbon optical properties at 9 regional background sites across Europe, *Atmos. Environ.*, 145, 346–364, <https://doi.org/10.1016/j.atmosenv.2016.09.035>, 2016.
- 850 Zhang, S., Tison, E., Dusanter, S., Beaugard, C., Gengembre, C., Augustin, P., Fourmentin, M., Delbarre, H., Riffault, V., 2021. Near real-time PM₁ chemical composition measurements at a French urban background and coastal site under industrial influence over more than a year: Temporal variability and assessment of sulfur-containing emissions. *Atmos. Environ.* 244, 117960. <https://doi.org/10.1016/j.atmosenv.2020.117960>



Zhang, Y., Favez, O., Albinet, A., Canonaco, F., Truong, F., Amodeo, T., Prevot, A., Sciare, J., and Gros, V.: Long-term measurements of the chemistry and sources of submicron aerosols at SIRTa in Paris area, France, in: European Aerosol Conference (EAC 2017), Zurich, Switzerland, 2017.

- 855 Zhang, Y., Favez, O., Petit, J.-E., Canonaco, F., Truong, F., Bonnaire, N., Cretn, V., Amodeo, T., Prévôt, A. S. H., Sciare, J., Gros, V., and Albinet, A.: Six-year source apportionment of submicron organic aerosols from near-continuous highly time-resolved measurements at SIRTa (Paris area, France), *Atmospheric Chem. Phys.*, 19, 14755–14776, <https://doi.org/10.5194/acp-19-14755-2019>, 2019.